Title

4π-spherically focused electromagnetic wave: diffraction optics approach and high-power limits.

Journal

Optics Express, 28(9)

ISSN

1094-4087

Authors

Jeong, Tae Moon

Bulanov, Sergei Vladimirovich

Sasorov, Pavel Vasilievich

et al.

Publication Date

2020-04-27

DOI

10.1364/oe.387654

Peer reviewed

Research Article | Vol. 28, No. 9 / 27 April 2020 / Optics Express 13991
Optics EXPRESS

4π-spherically focused electromagnetic wave: diffraction optics approach and high-power limits

TAE MOON JEONG,[1,*] SERGEI VLADIMIROVICH BULANOV,[1,2,3] PAVEL VASILIEVICH SASOROV,[1] STEPAN SERGEEVICH BULANOV,[4] JAMES KEVIN KOGA,[2] AND GEORG KORN[1]

[1]*Institute of Physics of the ASCR, ELI-Beamlines, Na Slovance 2, 18221 Prague, Czech Republic*
[2]*Kansai Photon Research Institute, National Institutes for Quantum and Radiological Science and Technology, 8-1-7 Umemidai, Kizugawa-shi, Kyoto 619-0215, Japan*
[3]*A. M. Prokhorov Institute of General Physics, the Russian Academy of Sciences, Vavilova 38, 119991 Moscow, Russia*
[4]*Lawrence Berkeley National Laboratory, Berkeley, California 94720, USA*
[*]*taemoon.jeong@eli-beams.eu*

Abstract: The focused field and its intensity distribution achieved by the 4π-spherical focusing scheme are investigated within the framework of diffraction optics. Generalized mathematical formulas describing the spatial distributions of the focused electric and magnetic fields are derived for the transverse magnetic and transverse electric mode electromagnetic waves with and without the orbital angular momentum attribute. The mathematical formula obtained shows no singularity in the field in the focal region and satisfies the finite field strength and electromagnetic energy conditions. The 4π-spherical focusing of the transverse magnetic mode electromagnetic wave provides the highest field strength at the focus and the peak intensity reaches 10^{26} W/cm^2 for the laser power of 100 PW at 800 nm wavelength. As an example of using the mathematical formula, the electron-positron pair production via the Schwinger mechanism is analyzed and compared with previous results.

1. Introduction

Physical phenomenon, such as light-light scattering [1,2] and electron-positron pair (e^+-e^- pair) production [1,3], associated with the quantum electrodynamics of strong fields [4] is of great interest as the available laser intensities approach ~10^{24} W/cm^2 and beyond [5,6]. Although the Schwinger field ($E_S = m_e^2c^3 / e\hbar \simeq 1.32 \times 10^{16}$ V/cm, the corresponding laser intensity of ~2.3×10^{29} W/cm^2) is still far from the reach of the current laser technology, many interesting ideas [7–10] have been proposed to experimentally demonstrate quantum phenomenon with a relatively lower laser power. Frequently-used ideas to reduce the laser power required for quantum phenomenon include the tight-focusing [11], the counter-propagating laser beams [12] or even multiple laser beam focusing [10].

Another interesting idea for reducing the required laser power is to spherically focus a single laser beam as discussed in Refs. [13–16]. From an optical point of view, the 4π-spherical focusing scheme can be regarded as an extreme case of either multiple laser beam focusing (in which the number of beams approaches infinity) or tight focusing (in which the f-number approaches zero) scheme. Thus, the 4π-spherical focusing scheme provides a theoretical limit to the highest field strength achievable with a given laser power. The tightly-focused field distribution is expressed by vector diffraction integrals and in general numerically calculated. However, under a specific circumstance such as the dipole and multipole configurations in the focal region [17], the diffraction integral for the 4π-spherical focusing can be analytically integrable for the 4π

#387654 https://doi.org/10.1364/OE.387654
Journal © 2020 Received 9 Jan 2020; revised 7 Feb 2020; accepted 22 Feb 2020; published 24 Apr 2020

Optics EXPRESS

solid angle and the general solution is given by the superposition of the products of spherical Bessel functions and spherical harmonics. Recently, Gonoskov and others have used this idea and developed the dipole pulse theory to describe the field distribution focused by the 4π-spherical focusing scheme [16]. In the theory, they also used a radially-polarized electromagnetic (EM) wave to maximize the field strength under the 4π-spherical focusing scheme. The use of radial polarization was successful because it can generate the most compact and highest field strength of the focused EM wave, which is different from the use of linear polarization which generates multiple intensity peaks appearing in the focal region. Thus, it becomes interesting to derive a general mathematical expression describing the 4π-spherically focused electric- (E-) and magnetic- (B-) field distributions within the framework of diffraction optics.

In order to apply the diffraction theory to the 4π-spherical focusing scheme, an incident EM wave should be focused by an ideal parabolic mirror with an extremely low f-number (f/# << 1), and then a surface on a virtual sphere located in between the parabolic mirror and the focus should be chosen as the entrance pupil. Finally, the field distribution projected on that virtual surface can be used to calculate the field distribution near the focus through diffraction theory. This approach is only valid when the wavelength of the EM wave is much smaller than the focal length of the parabolic mirror. In this approach, there are two different polarization states known as the transverse magnetic (TM) and transverse electric (TE) modes that can be chosen as the eigenstates (see [13] and references therein) under the 4π-spherical focusing scheme. The TM (TE) mode EM wave can be generated by 4π-spherically focusing the radially- (azimuthally-) polarized EM wave as shown in Fig. 1. The diffraction approach using a radially- (or azimuthally) polarized EM wave provides a mathematical formula describing the 4π-spherically focused field distribution for a TM (or TE) mode EM wave in the focal region. Recently, much attention has been paid to the use of orbital angular momentum (OAM) beams in laser-matter interaction studies [18–20]. The OAM can be imposed by introducing a helical phase profile to the EM wave [21]. Therefore, by imposing the OAM attribute to the EM wave, the diffraction approach can be used to extend the solution of field distribution for more general cases, such as beams with the OAM attribute. To have the exact expression for the focused OAM beam will be critical for studying laser-matter interactions using the OAM beams.

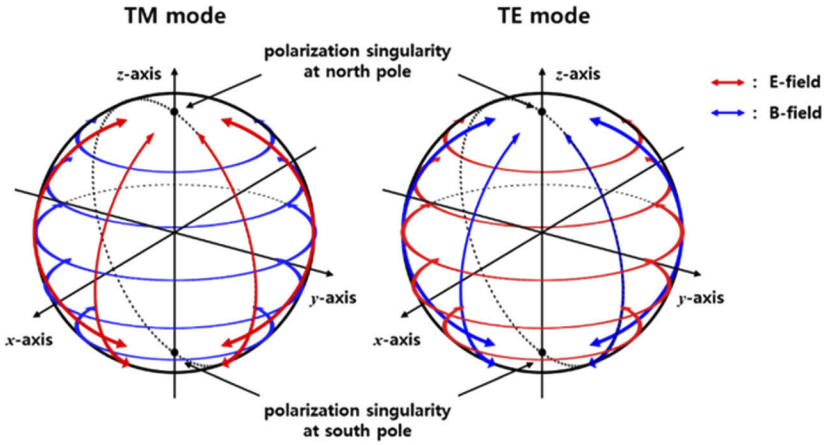

Fig. 1. Electric and magnetic field configurations for transverse magnetic (TM) and transverse electric (TE) modes. Because of the projected polarization singularities at the north (θ=0 rad) and south (θ=π rad) poles, the electric and magnetic fields should vanish at the poles of the spherical surface. For the TM mode, the E-field oscillates along the θ-direction and the B-field does along the ϕ-direction. In contrast, for the TE mode, the E-field oscillates along the ϕ-direction and the B-field along the θ-direction.

Optics EXPRESS

In this paper, the electromagnetic field distribution by the 4π-spherical focusing scheme has been investigated. Through the diffraction optic theory, generalized mathematical expressions describing E- and B-field distributions under the 4π-spherical focusing condition were derived for the TM and TE mode EM waves with and without the OAM attribute. The maximum achievable electric field strength is obtained with the conventional TM mode EM wave and the peak intensity reaches $\sim 10^{26}$ W/cm^2 for a 100 PW laser pulse at 800 nm wavelength. As an example of using the mathematical formulas, the e^+-e^- pair production rate is investigated with the formulas and the minimum laser power required for the pair production is estimated from the derived formulas and compared to previous results.

2. Electric and magnetic fields under 4π-spherical focusing scheme

2.1. Field solution for the 4π-spherically focused wave in the region of $kr >> 1$

The propagation of an EM wave is described by the Helmholtz' equation by

$$\nabla^2\vec{A} - \frac{1}{c^2}\frac{\partial^2}{\partial t^2}\vec{A} = 0. \tag{1}$$

Here, $\vec{A}$ is the vector potential. In spherical coordinates, the solution of Eq. (1) of which the field is far from the origin (kr >>1) is given by

$$A_\perp(k) = a(k)\sum_{n=0}^{\infty}\sum_{l=-n}^{n} j_n(kr)Y_n^l(\theta,\phi)\exp(-i\omega t). \tag{2}$$

Here, $j_n(kr)$ is the spherical Bessel function with a radial order of n and $Y_n^l(\theta,\phi)$ is the spherical harmonics of the n-th polar and l-th azimuthal orders. The function, $a(k)$, is the strength of the vector potential at the wavevector, k, and the angular frequency, ω, corresponds to $\omega = kc$. Because an ideal case (no wavefront aberration) of the spherical focusing is assumed, $A_\perp(k)$ represents the vector potential perpendicular to the radial direction. Considering the smallest focal spot under the spherical focusing scheme, the lowest order ($n = 0$ and $l = 0$) of the vector potential, $A_\perp(k) = a(k)\frac{\sin(kr)}{kr}\exp(-i\omega t)$, can be taken as a solution at kr>>1. As mentioned in the introduction, two eigen polarization states, A_θ and A_ϕ, are possible for the polarization of the vector potential. These polarization states correspond to the TM and TE modes in the focal region, respectively. The A_θ and A_ϕ have polarization singularities with a Poincaré-Hopf index of 1 at the north and south poles as shown in Fig. 1, and in this case there is no field strength for A_θ and A_ϕ at the polarization singularity. Therefore, the possible vector potentials for the TM and TE modes should have mathematical forms as,

$$\vec{A}(k) = a(k)\frac{\sin(kr)}{kr}\sin\theta\exp(-i\omega t)\hat{\theta}, \quad \text{(for TM mode)} \tag{3}$$

$$\text{and} \quad \vec{A}(k) = a(k)\frac{\sin(kr)}{kr}\sin\theta\exp(-i\omega t)\hat{\phi}. \text{ (for TE mode)} \tag{4}$$

The resultant E- and B-fields for the TM and TE modes are expressed as

$$\vec{E}(k) = ika(k)\frac{\sin(kr)}{kr}\sin\theta\exp(-i\omega t)\hat{\theta} \text{ and } \vec{H}(k) = \frac{ika(k)}{c}\frac{\sin(kr)}{kr}\sin\theta\exp(-i\omega t)\hat{\phi} \quad \text{(for TM mode)} \tag{5}$$

$$\vec{E}(k) = ika(k)\frac{\sin(kr)}{kr}\sin\theta\exp(-i\omega t)\hat{\phi} \text{ and } \vec{H}(k) = -\frac{ika(k)}{c}\frac{\sin(kr)}{kr}\sin\theta\exp(-i\omega t)\hat{\theta}. \quad \text{(for TE mode)} \tag{6}$$

Because of $\sin(kr) = \frac{e^{ikr}-e^{-ikr}}{2i}$, Eqs. (3)–(6) represent the superposition of incoming (-ikr) and outgoing (+ikr) spherical waves in the spherical focusing geometry, and the angular dependency

Optics EXPRESS

$(\sin\theta)$ results in EM fields by dipole radiation when $kr \gg 1$. These equations well explain the E- and B-field distributions when the observation point is far from the focus located at the origin. The E- and B-fields expressed in Eqs. (3)–(6) satisfy the finite condition for the field strength and the electromagnetic energy even with the distance from the origin approaching zero. However, the fields in Eqs. (3)–(6) are always zero at $\theta = 0$ even in a very short distance below one wavelength away from the focus. This sounds unphysical because, considering the diffraction effect of the focused EM wave, the field should exist within a very short range even at $\theta = 0$ and vanish quickly as the observation distance increases from the focus. Thus, the key question for the 4π-spherical focusing scheme becomes how to accurately express the physical E- and B-field distributions near the focus at $kr < 1$.

2.2. Field solution for the 4π-spherically focused wave in the region of $kr < 1$

In order to obtain the E- and B-field distributions for TM and TE mode EM waves near the focus, let us consider that a radially- or azimuthally-polarized EM wave with a Laguerre-Gaussian (LG) beam profile is incident on a parabolic mirror and focused by it (see Fig. 2). The Bessel-Gaussian (BG) function [22] is the general expression for the cylindrical vector beams such as radially-polarized (TM) and azimuthally-polarized (TE) EM wave. However, in the small-scale parameter limit [23], the beam profile follows the LG function [$E \sim LG_0^1 \sim (\rho/\rho_0)\exp(-\rho^2/2\rho_0^2)$]. Here, LG_0^1 means the LG function with 0th radial and 1st azimuthal orders. The parabolic surface profile is defined by $z = (x^2 + y^2)/4f - f$ with a parent focal length of f. The EM wave propagates along the -z-direction and it is reflected by the parabolic mirror to form the E-field distribution expressed by Eq. (5) onto a virtual focusing sphere (VFS).

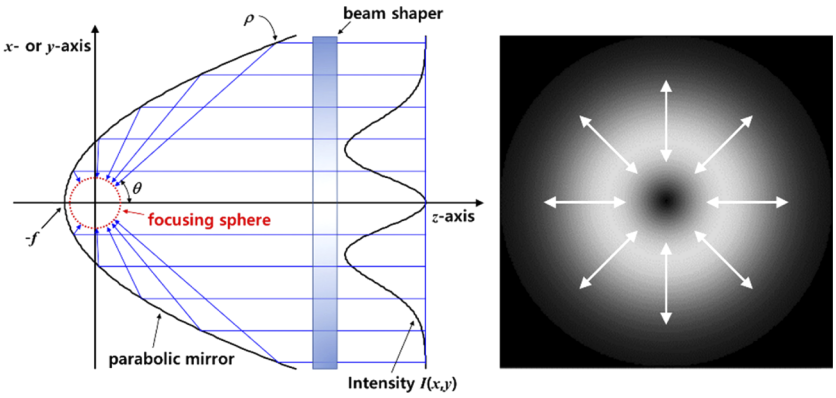

Fig. 2. (a) Schematics for projecting a radially-polarized electromagnetic wave onto the virtual focusing sphere with the electric field distribution of ~sinθ. (b) Transverse intensity distribution I(x,y) and polarization state of the incident radially-polarized electromagnetic wave.

The distance, ρ, in polar coordinates is defined as $\rho = r\sin\theta$ with $\rho = \sqrt{x^2 + y^2}$ and ρ_0 means the Gaussian beam size. It is also known that a general solution for the E-field profile of the OAM beam with a topological charge (TC) of α is given by

$$E \sim LG_0^\alpha \sim (\rho/\rho_0)^\alpha \exp(-\rho^2/2\rho_0^2) L_0^\alpha(\rho^2/\rho_0^2) e^{i\alpha\phi}. \tag{7}$$

Therefore, the beam profile becomes the LG_0^1 function when the TC equals to 0, ±1. The LG_0^1 beam mode does not match the beam profile shown in Eqs. (3)–(6). However, the required beam profile can be obtained by the coherent beam shaping technique [24,25]. With a proper beam

Optics EXPRESS

shaper which introduces the transmittance function of $\exp(\rho^2 / 2\rho_0^2) / r$ to the LG_0^1 mode, one can obtain the E-field distribution proportional to

$$E_S(\theta, \phi) \sim \sin\theta \cdot e^{i\alpha\phi} \tag{8}$$

on the VFS, as shown in Eqs. (5) and (6). Here, $r = \sqrt{x^2 + y^2 + z^2}$ is the radial distance and θ the polar angle in spherical coordinates. The TC (α) for the OAM of the EM wave in Eq. (8) is allowed to have 0 and ±1. A different beam shaper will be used for a beam with a higher TC. After being reflected by the parabolic mirror, the ρ-polarization of the EM wave in cylindrical coordinates turns into θ-polarization in spherical coordinates.

Now, using the diffraction technique introduced in [26], the E-field at the observation position, O, located near to the focus can be calculated by (see Fig. 3 for details)

$$d\vec{E}_O(r_O, \theta_O, \phi_O) = \frac{ik}{2\pi}\vec{E}_S(\theta_S, \phi_S)\frac{\exp(i\vec{k}\cdot\vec{u})}{|\vec{u}|}dA, \tag{9}$$

where (r_O, θ_O, ϕ_O) refers to the spherical coordinates of the observation point, $E_S(\theta_S, \phi_S)$ refers to the E-field at the source point (r_S, θ_S, ϕ_S) on the VFS, and dA the infinitesimal area of the source point. The $\vec{u}$ is the distance vector from the source point to the observation point. The phase factor, $\vec{k}\cdot\vec{u}$, refers to the incoming wave and is expressed as $\vec{k}\cdot\vec{u} = ku = k(r_S^2 + r_O^2 - 2r_S r_O\cos\gamma)^{1/2}$.

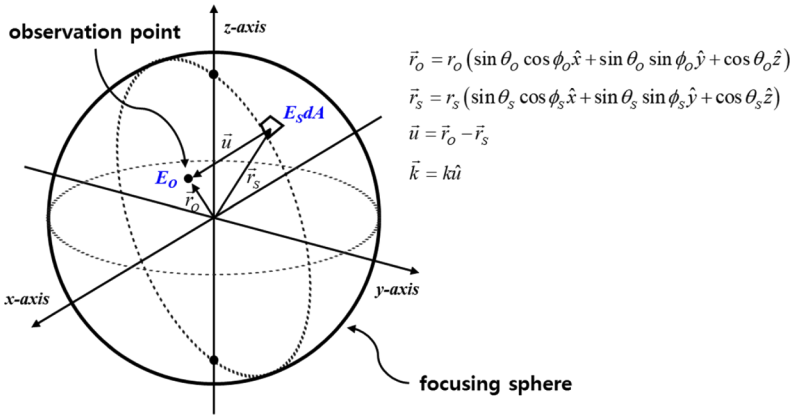

Fig. 3. Geometric configuration for diffraction integral under the 4π spherical focusing scheme.

Here, γ is the angle between two vectors ($\vec{r}_S$ and $\vec{r}_O$) to the source and the observation points, and $\cos\gamma$ is defined by $\cos\gamma = \cos\theta_S\cos\theta_O\cos(\phi_S - \phi_O) + \sin\theta_S\sin\theta_O$. By assuming $|r_S| \gg |r_O|$, the phase factor in Eq. (9) is approximated as $\vec{k}\cdot\vec{u} \approx kr_S - kr_O\cos\gamma$ and the distance, $|\vec{u}|$, in the denominator in Eq. (9) becomes $|\vec{u}| \approx r_S$ because the change in the field strength is slower than that in the phase. Then, the resultant expression for the electric field at the observation point is

$$\vec{E}_O(r_O, \theta_O, \phi_O) \approx \frac{ikr_S}{2\pi}\exp(ikr_S)\int \vec{E}_S(\theta_S, \phi_S)\exp(-ikr_O\cos\gamma)\sin\theta_S d\theta_S d\phi_S. \tag{10}$$

Equation (10) can be analytically integrable for the 4π solid angle by inserting $\vec{E}_S(\theta_S, \phi_S) = E_S\sin\theta_S\cdot\exp(i\alpha\phi_S)\hat{\theta}$ (for the TM mode) or $\vec{E}_S(\theta_S) = E_S\sin\theta_S\cdot\exp(i\alpha\phi_S)\hat{\phi}$ (for the TE mode) as an E-field at the source point. The field strength, E_S, on the VFS is obtained directly from the incident power, P_L, of the incoming EM wave or laser by using the energy conservation between

Optics EXPRESS

the incident laser power and the laser power on the VFS with a radius r_S. This conservation condition yields $\eta P_L = \pi c\varepsilon_0 r_S^2 E_S^2 \int_0^\pi \sin^3\theta_S d\theta_S$. Here, η is used to express the transmission of the beam shaper. Then, the E-field strength (E_S) on the VFS is given by $\sqrt{3\eta P_L / 4\pi c\varepsilon_0 r_S^2}$.

2.3. Field solution for the TM and TE mode waves in the region of $kr < 1$

Now, let us calculate the E-field distribution for the TM mode EM wave using Eq. (10). With the E-field profile [$\vec{E}_S(\theta_S, \phi_S) = E_S \sin\theta_S \cdot \exp(i\alpha\phi_S)\hat{\theta}$] on the VSF, Eq. (10) is re-written as

$$\vec{E}_O = \hat{\theta}E_O = \hat{\theta}\frac{ikr_S}{2\pi}E_S \exp(ikr_S)\int \exp(-ikr_O\cos\gamma)\exp(-i\alpha\phi_S)\sin^2\theta_S d\theta_S d\phi_S. \tag{11}$$

By the plane wave expansion of $\exp(-ikr_O\cos\gamma) = \sum_{l=0}^{\infty}(2l+1)(-i)^l j_l(kr_O)P_l(\cos\gamma)$ and the addition theorem of the Legendre function of $P_l(\cos\gamma) = \sum_{m=-l}^{l}\frac{\Gamma(l-m+1)}{\Gamma(l+m+1)}P_l^m(\cos\theta_O)P_l^m(\cos\theta_S)\exp[im(\phi_O-\phi_S)]$, the phase factor, $\exp(-ikr_O\cos\gamma)$, in Eq. (11) can be re-expressed as

$$\sum_{l=0}^{\infty}(2l+1)(-i)^l j_l(kr_O)\sum_{m=-l}^{l}\frac{\Gamma(l-m+1)}{\Gamma(l+m+1)}P_l^m(\cos\theta_O)P_l^m(\cos\theta_S)\exp[im(\phi_O-\phi_S)], \tag{12}$$

with the associated Legendre polynomials, P_l^m. After the straightforward mathematical calculations, the resultant E-field near the focus is finally given by

$$\begin{aligned}\vec{E}_O = {} & \hat{\theta}ikr_S E_S \exp(ikr_S)\exp(i\alpha\phi_O)\times \\ & \sum_{l=0}^{\infty}(2l+1)(-i)^l j_l(kr_O)\frac{\Gamma(l-\alpha+1)}{\Gamma(l+\alpha+1)}P_l^\alpha(\cos\theta_O)\int P_l^\alpha(\cos\theta_S)\sin^2\theta_S d\theta_S.\end{aligned} \tag{13}$$

Here, the integral formula of $\int_0^{2\pi}\exp[i(\alpha-m)\phi_S]d\phi_S = 2\pi\delta_{m,\alpha}$ is used to obtain Eq. (13) and $\Gamma(\cdot)$ is the gamma function. The integral, $\int_0^\pi P_l^\alpha(\cos\theta_S)\sin^2\theta_S d\theta_S$, is converted into $\int_{-1}^{1}P_l^\alpha(x)(1-x^2)^{1/2}dx$ and, under the condition of $\alpha < 3$, it can be explicitly expressed by the formula in [27] as follows:

$$\int_{-1}^{1}(1-x^2)^{\lambda-1}P_l^\alpha(x)dx = \frac{\pi 2^\alpha\Gamma(\lambda+\alpha/2)\Gamma(\lambda-\alpha/2)}{\Gamma(\lambda+l/2+1/2)\Gamma(\lambda-l/2)\Gamma(-\alpha/2+l/2+1)\Gamma(-\alpha/2-l/2+1/2)}. \tag{14}$$

Finally, putting Eq. (14) into Eq. (13), the general expression for the resultant E-field distribution in the focal region is expressed in the summation of the product of the spherical Bessel functions and the associated Legendre polynomials as

$$\begin{aligned}\vec{E}_O = {} & \hat{\theta}2^\alpha\pi ikr_S E_S \exp(ikr_S)\exp(i\alpha\phi_O)\Gamma(3/2+\alpha/2)\Gamma(3/2-\alpha/2)\times \\ & \sum_{l=0}^{\infty}\frac{(2l+1)(-i)^l\Gamma(l-\alpha+1)j_l(kr_O)P_l^\alpha(\cos\theta_O)}{\Gamma(l+\alpha+1)\Gamma(l/2+2)\Gamma(3/2-l/2)\Gamma(-\alpha/2+l/2+1)\Gamma(-\alpha/2-l/2+1/2)}.\end{aligned} \tag{15}$$

In case of the conventional EM wave with a TC of α=0, the E-field distribution near the focus can be written with the first three non-zero terms as follows:

$$\begin{aligned}\vec{E}_O &= \hat{\theta}i\frac{\pi}{2}kr_S E_S \exp(ikr_S)\left[j_0(kr_O) + \frac{5}{2^3}j_2(kr_O)P_2(\cos\theta_O) - \frac{9}{2^6}j_4(kr_O)P_4(\cos\theta_O) + \cdots\right] \\ &= \hat{\theta}iE_p \exp(ikr_S)a(r_O,\theta_O).\end{aligned} \tag{16}$$

Optics EXPRESS

Here, E_p is the peak of E-field strength defined by $\pi k r_S E_S/2$ and $a(r_O, \theta_O)$ is the spatial distribution function of the E-field given by

$$a(r_O, \theta_O) = \left[j_0(kr_O) + \frac{5}{2^3} j_2(kr_O) P_2(\cos\theta_O) - \frac{9}{2^6} j_4(kr_O) P_4(\cos\theta_O) + \cdots \right]. \tag{17}$$

Because the phase shift, kr_S, is a constant, $\exp(ikr_S)$ can be dropped out without the loss of generality at any time. Equation (16) is a physical solution for the E-field distribution of a spherically focused TM mode EM wave near the focus ($kr < 1$) because the field has a non-zero value even if the radius r_O and the polar angle θ_O approach zero. The temporal characteristics can be obtained by multiplying by the phase factor of $e^{-i\omega t}$. The E-field distribution and its temporal characteristics are shown in Figs. 4(a) and 4(b). The first two terms in Eq. (17) are used to calculate the field distribution near the focus. The wavelength of the incoming EM wave is 0.8 μm. The field distribution forms a standing wave near the focus and oscillates with respect to time as in the figures. The line-cut of the field distribution showed a rapid decrease along the z-axis as expected. The zeros of the E- field are obtained at 0.5 μm (0.63λ) and 0.37 μm (0.46λ) in the z- and x- (or y-) axes, respectively. The FWHMs of $a^2(r_O, \theta_O)$ in the z- and x-axes are 0.21 μm (0.26λ) and 0.17 μm (0.21λ), yielding the FWHM volume of $(4\pi/3) \times 0.26 \times 0.21 \times 0.21\lambda^3 \approx \lambda^3/20$.

For the 4π-spherically-focused OAM EM wave with a TC of α=±1, the $l = 1$ term in Eq. (15) only survives due to the gamma function properties of $\Gamma(0) = \infty$ and $\Gamma(-|\text{int}|) = \infty$ in the denominator. Therefore, the focused field distribution for the OAM EM wave with a TC of ±1 becomes

$$\vec{E}_O = -\hat{\theta}\frac{4}{\pi} E_p \exp(ikr_S) \exp(\pm i\phi_O) j_1(kr_O) P_1^1(\cos\theta_O). \tag{18}$$

Figures 4(c) and 4(d) show the field distribution and its temporal characteristics for the 4π-spherically-focused EM wave with a TC of 1. The helical phase property appears in the focused field, thus the field distribution in the focal region rotates in the ϕ-direction with respect to time as shown in Fig. 4(d).

The focused E-field distribution of the TE mode EM wave can be calculated by inserting $\vec{E}_S(\theta_S, \phi_S) = E_S \sin\theta_S \cdot \exp(i\alpha\phi_S)\hat{\phi}$ into Eq. (10). In this case, it is convenient to separately calculate the x- and y-polarization components by using $\hat{\phi} = -\sin\phi_S\hat{x} + \cos\phi_S\hat{y}$. The x- and y-polarization components are given by

$$E_{O,x} = -\frac{kr_S}{4\pi} E_S \exp(ikr_S)[I_+ - I_-], \text{ and } E_{O,y} = \frac{ikr_S}{4\pi} E_S \exp(ikr_S)[I_+ + I_-] \tag{19}$$

with the definition of $I_\pm = \int \exp(-ikr_O \cos\gamma) \exp[-i(\alpha \pm 1)\phi_S] \sin^2\theta_S d\theta_S d\phi_S$. By performing the integration in the ϕ_S-direction, $I_\pm$ become

$$I_\pm = 2\pi \sum_{l=0}^{\infty} (2l+1)(-i)^l j_l(kr_O) \frac{\Gamma[l-(\alpha\pm1)+1]}{\Gamma[l+(\alpha\pm1)+1]} P_l^{\alpha\pm1}(\cos\theta_O) e^{i(\alpha\pm1)\phi_O} \int P_l^{\alpha\pm1}(\cos\theta_S) \sin^2\theta_S d\theta_S. \tag{20}$$

Again, the focused field distribution for the conventional TE mode EM wave with no OAM attribute is obtained with α=0. In this case, by using the integration formulas [25] for odd ls, the integration in Eq. (20) becomes

$$\int_0^\pi P_l^{-1}(\cos\theta_S) \sin^2\theta_S d\theta_S = 2\frac{2^{-2}\Gamma(1/2)\Gamma(1)}{\Gamma(3/2-l/2)\Gamma(2+l/2)}, \tag{21}$$

$$\text{and } \int_0^\pi P_l^1(\cos\theta_S) \sin^2\theta_S d\theta_S = 2\frac{(-1)2^{-2}\Gamma(1/2)\Gamma(1)\Gamma(2+l)}{\Gamma(l)\Gamma(3/2-l/2)\Gamma(2+l/2)}. \tag{22}$$

All other ls become zeros except for $l = 1$ in Eqs. (21) and (22). Thus, the integrals, I_+ and I_-, become $4\pi i \cdot j_1(kr_O) P_1^1(\cos\theta_O) e^{i\phi_O}$ and $-8\pi i \cdot j_1(kr_O) P_1^{-1}(\cos\theta_O) e^{-i\phi_O}$, respectively. By

Optics EXPRESS

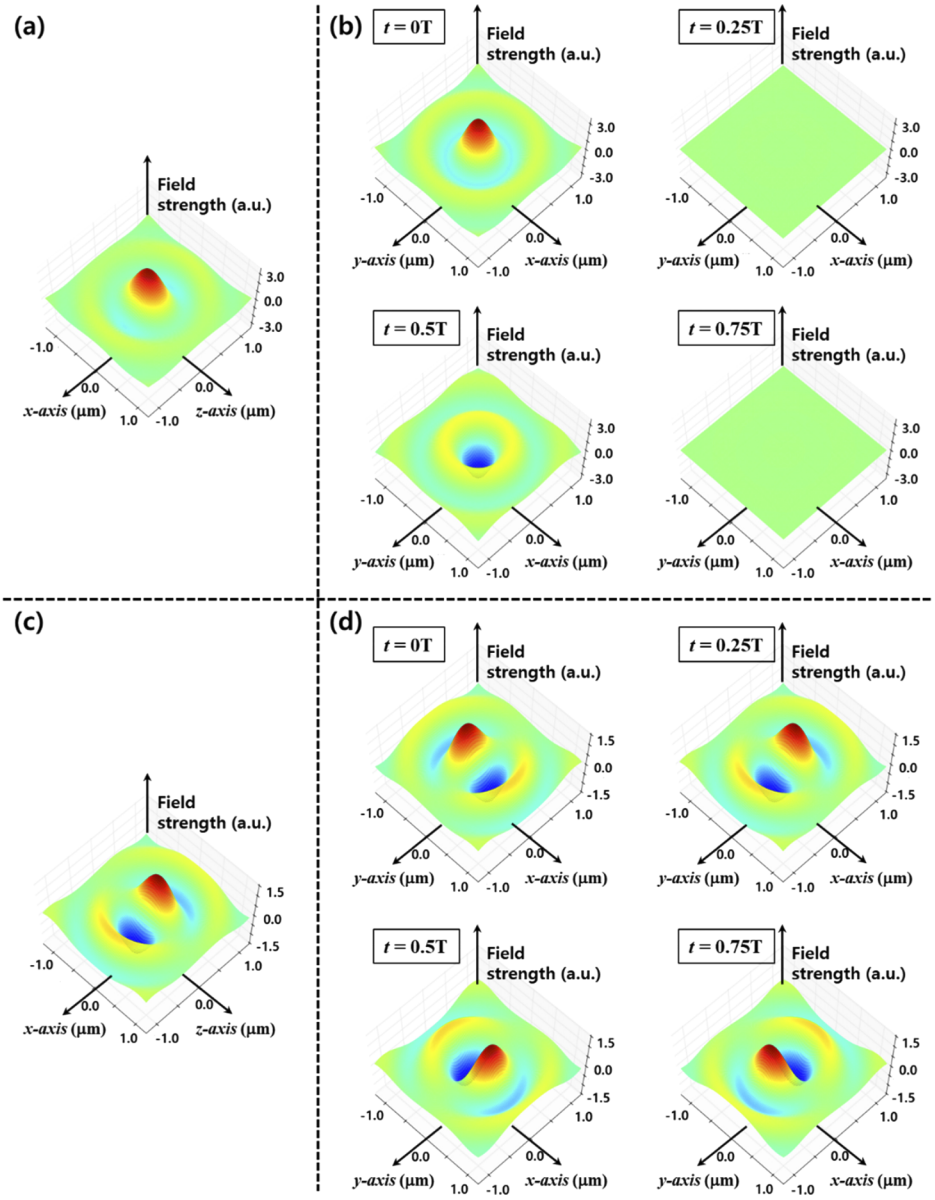

Fig. 4. Electric field distributions for the conventional and OAM TM mode EM waves. (a) and (c) show the field distributions for the conventional and OAM waves in the x-z plane. (b) and (d) show the field distributions for the conventional and OAM waves in the x-y plane at different times. For the conventional wave, the field oscillates in time. The OAM wave rotates in time along the z-axis. In (b) and (d), T in the figure means the period.

Optics EXPRESS

putting these expressions into Eq. (19), one obtains the following for the x- and y-polarization components

$$E_{O,x} = 2krsE_S \exp(ikr_S) j_1(kr_O) P_1^1(\cos\theta_O) \sin\phi_O, \tag{23}$$

$$\text{and } E_{O,y} = -2krsE_S \exp(ikr_S) j_1(kr_O) P_1^1(\cos\theta_O) \cos\phi_O. \tag{24}$$

Finally, the 4π-spherically focused E-field distribution of a TE mode EM wave in the focal region becomes

$$\vec{E}_O = -\hat{\phi} 2krsE_S \exp(ikr_S) j_1(kr_O) P_1^1(\cos\theta_O) = -\hat{\phi} E_P \exp(ikr_S) b(r_O, \theta_O). \tag{25}$$

Again, the spatial distribution function of the E-field, $b(r_O, \theta_O)$, is defined by

$$b(r_O, \theta_O) = \frac{4}{\pi} j_1(kr_O) P_1^1(\cos\theta_O). \tag{26}$$

The E-field distribution and its temporal characteristics are shown in Figs. 5(a) and 5(b). As shown in the figures, the E-field has zero field at the focus and its distribution for the TE mode EM wave forms a standing wave again and oscillates with respect to time.

The OAM TE mode EM wave shows an interesting field distribution pattern in the focal region. For the OAM TE mode EM wave with a TC of α=1, the integrals, $I_{\pm}$, become

$$I_+ = 2\pi \sum_{l=0}^{\infty} (2l+1)(-i)^l j_l(kr_O) \frac{\Gamma[l-1]}{\Gamma[l+3]} P_l^2(\cos\theta_O) e^{i2\phi_O} \int P_l^2(\cos\theta_S) \sin^2\theta_S d\theta_S, \tag{27}$$

$$\text{and } I_- = 2\pi \sum_{l=0}^{\infty} (2l+1)(-i)^l j_l(kr_O) P_l^0(\cos\theta_O) \int P_l^0(\cos\theta_S) \sin^2\theta_S d\theta_S. \tag{28}$$

The integrals can be explicitly expressed up to the second radial order as follows:

$$I_+ \approx 2\pi \frac{5 \cdot 3\pi}{2^6} \cdot j_2(kr_O) \cdot P_2^2(\cos\theta_O) e^{i2\phi_O}, \tag{29}$$

$$\text{and } I_- \approx 2\pi \left[\frac{1}{2}\pi j_0(kr_O) P_0^0(\cos\theta_O) + \frac{5}{2^4}\pi j_2(kr_O) P_2^0(\cos\theta_O) \right]. \tag{30}$$

Finally, the focused field distributions for the x- and y-polarization components in Eq. (19) become

$$E_{O,x} \approx -\frac{kr_S}{2} E_S \exp(ikr_S) \frac{\pi}{2} \left[\frac{3 \cdot 5}{2^5} j_2(kr_O) \cdot P_2^2(\cos\theta_O) e^{i2\phi_O} - j_0(kr_O) \right], \tag{31}$$

$$\text{and } E_{O,y} \approx \frac{kr_S}{2} E_S \exp(ikr_S) \frac{\pi}{2} \left[\frac{3 \cdot 5}{2^5} j_2(kr_O) \cdot P_2^2(\cos\theta_O) e^{i2\phi_O} + j_0(kr_O) \right]. \tag{32}$$

The $E_{O,x}$ field distribution of the TE mode OAM EM wave and its temporal characteristics are shown in Figs. 5(c) and 5(d). The field distribution in the focal region represents the superposition of two azimuthal modes (α+1 = 2 and α-1 = 0) due to the polarization-phase coupling as discussed in [28]. And, because of the helical phase shift of $e^{i2\phi_O}$, the field distribution in the focal region rotates in the ϕ-direction with respect to time.

The expression for the magnetic field distribution near the focus can be easily obtained by exchanging the field expressions for the E- and B-fields between TM and TE modes. The E-field configuration of the TM mode EM wave corresponds to B-field of the TE mode EM wave and vice versa. Thus, the B-field distribution for the TM mode EM wave in the focal region will be the same as the E-field distribution of TE mode EM wave. Similarly, the B-field distribution for

Optics EXPRESS

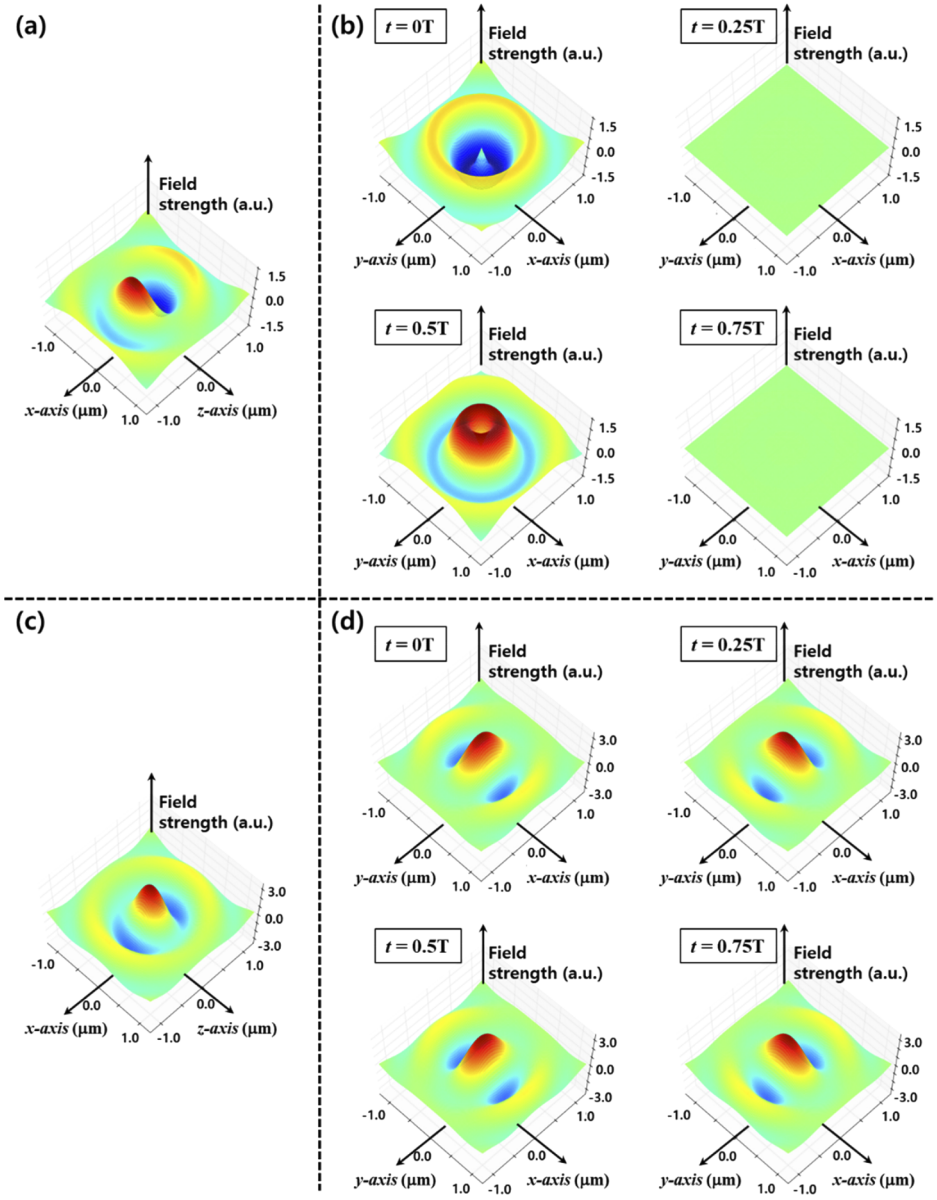

Fig. 5. Electric field distributions for the conventional and OAM TE mode EM waves. (a) and (c) show the field distributions for the conventional and OAM waves in the x-z plane. (b) and (d) show the field distributions for the conventional and OAM waves in the x-y plane at different times. For the conventional wave, the field oscillates in time. The OAM wave rotates in time along the z-axis. In (b) and (d), T in the figure means the period.

Optics EXPRESS

the TE mode EM wave will be the same as the E-field distribution of the TM mode EM wave. Therefore, the magnetic field distributions for the conventional EM waves are

$$\vec{H}_O = -\hat{\phi}\frac{E_P}{c}\exp(ikr_S)b(r_O,\theta_O) \quad \text{(for TM mode)} \tag{33}$$

$$\text{and } \vec{H}_O = \hat{\theta}i\frac{E_p}{c}\exp(ikr_S)a(r_O,\theta_O). \quad \text{(for TE mode)} \tag{34}$$

For the OAM EM wave, the B-field for the TM mode will be expressed with Eqs. (31) and (32) and the B-field for the TE mode with Eq. (18). Equations (16), (18), (25), (31), and (32) form a full set of expressions describing 4π-spherically focused E- and B-field distributions for the conventional (α=0) and OAM (α=±1) TM/TE mode EM waves.

2.4. Attainable highest peak field strength and intensity

As mentioned before, the highest E-field strength defined by $\frac{\pi}{2}kr_SE_S$ is obtained for the conventional TM mode EM wave at r_O=0. By replacing E_S with $\sqrt{3\eta P_L/4\pi c\varepsilon_0 r_S^2}$, one obtains the peak of field strength and the peak intensity at the focus as follows:

$$E_p = \frac{k}{4}\sqrt{\frac{3\pi\eta P_L}{c\varepsilon_0}} \text{ and } I_p = \frac{3\pi^3}{4}\frac{\eta P_L}{\lambda^2} \tag{35}$$

Table 1 shows the peak intensity and field strength calculated at various powers and wavelengths. In the table, the 1-μm wavelength laser represents a 150-fs high-power Nd:glass laser and the 0.8-μm wavelength laser for a 30-fs Ti:sapphire laser [5]. The different wavelengths such as 0.5 μm, 0.4 μm, and 0.2 μm can be obtained by the second and fourth harmonic generations of these lasers [29]. The table shows that the peak intensity of $\sim 1.8\times10^{24}$ W/cm^2 can be theoretically reached by spherically focusing a 1 PW Ti:sapphire laser pulse. It is interesting to note that such a high laser intensity can be achieved with a focused spot size of $\sim\lambda/2$ and that the spherical focusing scheme provides the $\lambda/2$-focusing condition, which is the limit of diffraction optics theory based on the wave-like property of light. At the same laser power, the field strength calculated with Eq. (35) provides a 1.18 times higher value than that calculated by the dipole pulse theory [16]. It is also worth examining the theoretical limit of achievable laser intensity by focusing 10 PW and 100 PW laser pulses. The spherical focusing of 10 PW and 100 PW laser pulses at the fourth harmonics pushes the peak intensities above 2.9×10^{26} W/cm^2 and 2.9×10^{27} W/cm^2, respectively. The intensity of 2.9×10^{27} W/cm^2 corresponds to the peak field strengths of 1.48×10^{15} V/cm, corresponding to 11.2% of the Schwinger field.

3. Electron-positron pair production under 4π-spherical focusing scheme

One of the purposes of having the mathematical expressions of the 4π-spherically focused EM wave is to investigate the e^+-e^- pair production under the ultra-strong EM field. In this section, the e^+-e^- pair production rate and the required laser power for a single e^+-e^- pair production event are estimated with the 4π-spherically focused EM field. The e^+-e^- pair production from the vacuum by the Schwinger mechanism [30] is a tunneling process, and under the constant field condition the total number ($N_{e^+e^-}$) of the created e^+-e^- pairss is calculated by [3,12,31,32],

$$N_{e^+e^-} = \int d^4x W_{e^+e^-} = \frac{e^2E_S^2}{4\pi^3\hbar^2c^2}\int d^4x E_{inv}H_{inv}\coth(\pi H_{inv}/E_{inv})\exp\left(-\frac{\pi}{E_{inv}}\right). \tag{36}$$

Here, E_{inv} and H_{inv} are the reduced invariants defined by

$$E_{inv} = \frac{\sqrt{(F^2+G^2)^{1/2}-F}}{E_S}, \text{ and } H_{inv} = \frac{\sqrt{(F^2+G^2)^{1/2}+F}}{E_S}, \tag{37}$$

Optics EXPRESS

where, F and G are the Poincaré invariants defined by $F = [H^2 - (E^2/c^2)]/2$ and $G = -[\vec{H}^* \cdot (\vec{E}/c) + (\vec{E}^*/c) \cdot \vec{H}]/2$. The e^+-e^- pair production rate, $W_{e^+e^-}$, which means the number of e^+-e^- pairss created in the four-volume d^4x, is given by

$$W_{e^+e^-} = \frac{e^2E_S^2}{4\pi^3\hbar^2c^2} E_{inv}H_{inv} \coth\left(\pi\frac{H_{inv}}{E_{inv}}\right)\exp\left(-\frac{\pi}{E_{inv}}\right). \tag{38}$$

Here, $\hbar$ is the Planck constant. Although Eq. (38) is valid for a constant field, its validity can be extended to the oscillating field through the locally constant field approximation, when the wavelength of the EM wave is much greater than the Compton wavelength [30].

In order to explicitly represent the Poincaré invariants with mathematical expressions for the fields, let us assume that a generalized conventional (α=0) EM wave expressed as the superposition of TM and TE mode EM waves with a phase difference of γ is spherically focused. Then, the E- and B-field are given as follows:

$$\vec{E} = E_p\begin{bmatrix} 0 \\ iR_1(t)a(r_O,\theta_O)\cos(\omega_1 t) \\ -R_2(t)e^{i\gamma}b(r_O,\theta_O)\cos(\omega_2 t)\end{bmatrix} \text{ and } \vec{H} = \frac{E_p}{c}\begin{bmatrix} 0 \\ iR_2(t)e^{i\gamma}a(r_O,\theta_O)\cos(\omega_2 t) \\ -R_1(t)b(r_O,\theta_O)\cos(\omega_1 t)\end{bmatrix}. \tag{39}$$

Here, $R_1(t)$ and $R_2(t)$ are used to express the temporal envelope of the EM waves and ω_1 and ω_2 are angular frequencies for the TM and TE mode EM waves. By putting the E- and B-field expressions in Eq. (38) into the expressions for the Poincaré invariants, one obtains

$$F(r_O,\theta_O,t) = -E_p^2 f(t)[a^2(r_O,\theta_O) - b^2(r_O,\theta_O)], \tag{40}$$

$$\text{and } G(r_O,\theta_O,t) = -E_p^2 g(t)[a^2(r_O,\theta_O) - b^2(r_O,\theta_O)]\sin\gamma \tag{41}$$

with the notation of $c = 1$. The $f(t)$ and $g(t)$ are the time-dependent functions defined as

$$f(t) = R_1^2(t)\cos^2(\omega_1 t) - R_2^2(t)\cos^2(\omega_2 t) \text{ and } g(t) = R_1(t)R_2(t)\cos\omega_1 t\cos\omega_2 t, \tag{42}$$

respectively. Under the locally constant field approximation of the pulse duration << the Compton time, the functions, $f(t)$ and $g(t)$, can be regarded as constants, f_0 and g_0, at a certain time t_0, so the Poincaré invariants become dependent only on the spatial coordinates. Figure 6 shows the spatial distribution function $(a^2(r_O,\theta_O) - b^2(r_O,\theta_O))$ appearing in the Poincaré invariants, F and G. The spatial distribution function, $a^2 - b^2$, has zero values at 0.23 μm, 0.47 μm, and 0.69 μm on the x- and y-axes, and at 0.50 μm, 0.88 μm, and 1.26 μm on the z-axis. The Poincaré invariant G is always zero when $R_1(t) = 0$, or $R_2(t) = 0$, or $\sin\gamma = 0$. In other cases, an invariant G is not zero and a Lorentz frame in which the E- and B-fields are parallel (or antiparallel) can be found.

Now, by inserting Eqs. (40) and (41) into Eq. (37), one obtains $E_{inv}H_{inv}$ and H_{inv}/E_{inv} as follows:

$$E_{inv}H_{inv} = \frac{2E_p^2(a^2-b^2)g_0\sin\gamma}{E_S^2} \text{ and } \frac{H_{inv}}{E_{inv}} = \frac{f_0}{2g_0\sin\gamma}\left(-1+\sqrt{1+\frac{4g_0^2}{f_0^2}\sin^2\gamma}\right). \tag{43}$$

Due to Eq. (35), the peak field strength, E_p, is inversely proportional to the wavelength of the EM wave, so that the pair-production rate $W_{e^+e^-}$ is proportional to $\frac{1}{\lambda^2}\exp(-C\lambda)$, where C is a constant. This result shows that using a shorter wavelength is beneficial in increasing the pair production rate and consistent with the previous result [32]. The method to obtain a shorter wavelength is to use high harmonics from a solid or gas target [33–35] and the reflection from

Optics EXPRESS

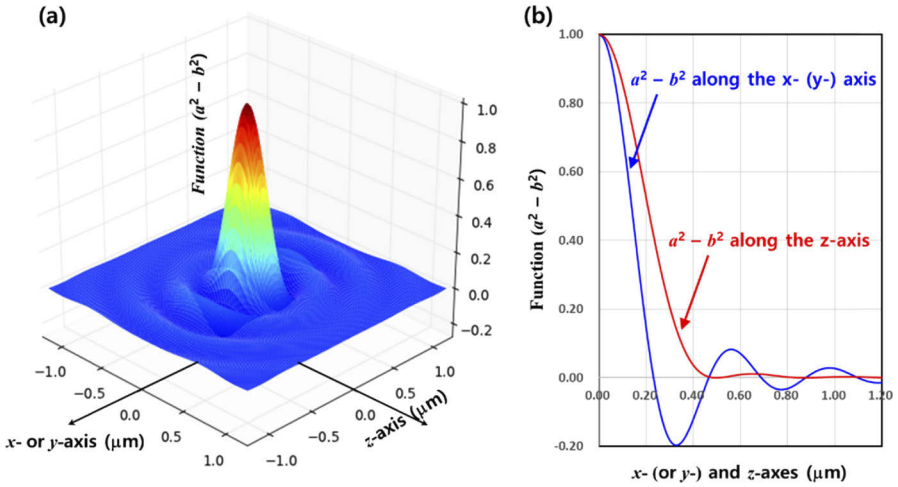

Fig. 6. (a) Spatial distribution and (b) line plot of the spatial function $(a^2 - b^2)$ of the Poincare invariants, F and G.

Table 1. Peak intensities and field strengths at the focus under various peak powers and wavelengths (when η=1). The 1 PW laser is currently operating worldwide, the 10 PW laser is under construction [4], and the construction of over 100 PW laser is planned [5].

		1 μm	0.8 μm	0.5 μm (2^{nd} harmonic of 1 μm)	0.4 μm (2^{nd} harmonic of 0.8 μm)	0.2 μm (4^{th} harmonic of 0.8 μm)
1 PW	Peak intensity (W/cm^2)	1.16×10^{24}	1.82×10^{24}	4.65×10^{24}	7.27×10^{24}	2.91×10^{25}
	Peak field strength (V/cm)	2.96×10^{13}	3.70×10^{13}	5.92×10^{13}	7.40×10^{13}	1.48×10^{14}
10 PW	Peak intensity (W/cm^2)	1.16×10^{25}	1.82×10^{25}	4.65×10^{25}	7.27×10^{25}	2.91×10^{26}
	Peak field strength (V/cm)	9.36×10^{13}	1.17×10^{14}	1.87×10^{14}	2.34×10^{14}	4.68×10^{14}
100 PW	Peak intensity (W/cm^2)	1.16×10^{26}	1.82×10^{26}	4.65×10^{26}	7.27×10^{26}	2.91×10^{27}
	Peak field strength (V/cm)	2.96×10^{14}	3.70×10^{14}	5.92×10^{14}	7.40×10^{14}	1.48×10^{15}

the relativistic flying mirror [36]. In particular, a very short wavelength, which is proportional to $1/(4\gamma^2)$, can be obtained from the reflected EM from a flying mirror due to the double Doppler effect. Moreover, special geometry of a plasma wake wave can produce spherical relativistic flying mirror for efficient light intensification by not only frequency up-conversion but also by spherical focusing [37].

Let's consider the pair production rate under three different modes of EM waves: TM mode, TE mode, and mixed TM/TE mode EM waves with the same angular frequency, i.e., $\omega_1 = \omega_2 = \omega$.

3.1. Pair production with the TM mode EM wave

For the TM mode EM wave, because $R_1 \gg R_2, f_0^2 \gg g_0^2$. The arguments ($H_{inv}/E_{inv}$ and $1/E_{inv}$) in the hyperbolic cotangent and exponential functions are approximated by

$$\frac{H_{inv}}{E_{inv}} \approx \frac{g_0 \sin\gamma}{f_0} \text{ and } \frac{1}{E_{inv}} \approx \frac{E_S}{E_p\sqrt{f_0(a^2-b^2)}}. \tag{44}$$

The time-dependent function, $f(t)$, is replaced by $f_0 = R_1^2(t_0)\cos^2(\omega t_0)$ under the locally-constant field approximation. By inserting Eq. (44) into Eq. (38), one obtains the pair production rate as

Optics EXPRESS

follows:

$$W_{e^+e^-} = \frac{e^2E_p^2}{4\pi^3\hbar^2c^2}\frac{R_1^2(t_0)\cos^2(\omega t_0)(a^2-b^2)}{\pi}\exp\left(-\frac{\pi E_S}{E_pR_1(t_0)\sqrt{\cos^2(\omega t_0)(a^2-b^2)}}\right). \quad (45)$$

The approximation of $\coth x \approx \frac{1}{x}$ is used when $x \ll 1$. The pair production occurs when $a^2 > b^2$ and its production peak appears twice in one optical cycle because of $\cos^2(\omega t)$. Table 2 shows the laser power required for the single event of e^+-e^- pair production in the four-volume. The pair production rate has significant values only near the peak field strength and rapidly decreases as the field strength decreases from the peak. In the table, it is assumed that an EM wave at the 0.2-μm wavelength is obtained from the fourth harmonic generation of a 0.8-μm Ti:sapphire high-power laser, an EM wave at the 0.04-μm wavelength is emitted from the higher-order harmonic generation in gas or solid target through the high-power laser-matter interaction, and an EM wave at the 0.002-μm wavelength is from the frequency-upshifted [38] EM wave reflected by the relativistic flying mirror. As can be seen in Table 2, when focusing the EM waves frequency-upshifted by the relativistic flying mirrors, the laser power required for the first event of e^+-e^- pair production is reduced to ~6 TW. The required laser powers are lower than those shown in the previous result [32] because of the higher field strength calculated with Eq. (35). However, the field strengths between two approaches differ by only 5%.

Table 2. Required peak power for the first event of electron-positron pair production under 4π-spherically focused TM mode EM wave.

Wavelength	1 μm	0.8 μm	0.2 μm (4^{th} harmonic of 0.8 μm)	0.04 μm (20^{th} harmonic of 0.8 μm)	0.002 μm ($4\gamma^2 = 400$)
Required peak power (PW)	1380	886	55.4	2.21	0.006

3.2. Pair production with the TE mode EM wave

For the TE mode EM wave, one obtains again $f_0^2 \gg g_0^2$ because $R_2 \gg R_1$. The arguments (H_{inv}/E_{inv} and $1/E_{inv}$) in the hyperbolic cotangent and exponential functions are the same as in Eq. (44). However, in this case, the function, f_0, becomes $-R_2^2(t)\cos^2(\omega t_0)$, and after a short calculation, the pair production rate for the TE mode EM wave case is given by

$$W_{e^+e^-} = \frac{e^2E_p^2}{4\pi^3\hbar^2c^2}\frac{R_2^2(t_0)\cos^2(\omega t_0)(b^2-a^2)}{\pi}\exp\left(-\frac{\pi E_S}{E_pR_2(t_0)\sqrt{\cos^2(\omega t_0)(b^2-a^2)}}\right). \quad (46)$$

Note that $b(r_O, \theta_O)$ means the E-field distribution for the TE mode EM wave. Because the pair production occurs only when $b^2 > a^2$, no pair production is expected at the focus (origin) where no E-field ($b = 0$) exists. The peak of pair production rate is obtained at $x = y \sim 0.425\lambda$, but, due to the lower E-field strength of the TE mode EM wave, the e^+-e^- pair production is much less than that with the TM mode EM wave.

3.3. Pair production with a mixed TM/TE mode EM wave

For the mixed TM/TE mode EM wave, the function, f_0, becomes zero and the other function, g_0, becomes $R^2(t_0)\cos^2\omega t_0$ with $R_1(t) = R_2(t) = R(t)$. Then, one obtains the following relations for

Optics EXPRESS

H_{inv}/E_{inv} and $1/E_{inv}$,

$$\frac{H_{inv}}{E_{inv}} = 1 \text{ and } \frac{1}{E_{inv}} = \frac{E_S}{E_p R(t_0)\cos(\omega t_0)\sqrt{(a^2-b^2)\sin\gamma}}. \tag{47}$$

By inserting Eq. (47) into Eq. (38), the pair production rate for the mixed TM/TE mode EM wave becomes

$$W_{e^+e^-} = \frac{e^2E_p^2}{4\pi^3\hbar^2c^2}R^2(t_0)(a^2-b^2)\sin\gamma\coth(\pi) \times \exp\left(-\frac{\pi E_S}{E_p R(t_0)\sqrt{\cos^2(\omega t_0)(a^2-b^2)\sin\gamma}}\right). \tag{48}$$

Equation (48) shows the pair production rate depending on the phase difference, γ, between TM and TE modes. The maximum pair production is obtained at the phase difference of $\gamma = \pi/2$, and no pair production is expected when $\gamma = 0$ or $\gamma = \pi$. Note that the constant factor of $1/\pi$ in Eqs. (45) and (46) is replaced by $\coth(\pi) \approx 1.003$. However, the e^+-e^- pair production rate will be much lower when comparing the E-field strengths in the mixed TM/TE mode and the TM mode EM wave.

4. Conclusion

The 4π-spherical focusing scheme has been investigated with the TM and TE mode EM waves through the diffraction optics approach. Due to the advantage of the diffraction optics approach, the mathematical expressions describing the 4π-spherically focused EM waves have been generalized to the OAM EM wave. The FWHM volume of the focused intensity is reduced to $\sim\lambda^3/20$ for the conventional TM mode EM wave and the peak intensity reaches 10^{27} W/cm^2 by focusing a 100 PW, 0.2-μm laser pulse, which will be available in the near future. The e^+-e^- pair production rate has been investigated under the 4π-spherical focusing condition. The pair production rate is analyzed for the TM, TE, and mixed TM/TE mode conventional EM waves. The required laser power for the e^+-e^- pair production reduces to the ~6 TW level by spherically focusing a TM mode EM wave reflected by a relativistic flying mirror. The result can be applied to investigate the nonlinear QED processes in the intensity range over 10^{24} W/cm^2.

Funding

European Regional Development Fund (CZ.02.1.01/0.0/0.0/15_003/0000449); U.S. Department of Energy Office of Science Offices of High Energy Physics and Fusion Energy Sciences (through LaserNetUS), under Contract No. DE-AC02-05CH1123.

Disclosures

The authors declare no conflicts of interest.

References

1. G. V. Dunne, "Heisenburg-Euler Effective Lagrangians: Basics and Extensions," in *From Fields to Strings: Circumnavigating Theoretical Physics*, M. Shifman, A. Vainshtein, and J. Wheater, eds. (World Scientific, 2005).
2. B. King and T. Heinzl, "Measuring Vacuum Polarisation with High Power Lasers," High Power Laser Sci. Eng. **4**, e5 (2016).
3. J. Schwinger, "On gauge invariance and vacuum polarization," Phys. Rev. **82**(5), 664–679 (1951).
4. A. Di Piazza, C. Muller, K. Z. Hatsagortsyan, and C. H. Keitel, "Extremely high-intensity laser interactions with fundamental quantum systems," Rev. Mod. Phys. **84**(3), 1177–1228 (2012).
5. ELI: http://www.extreme-light-infrastructure.eu/
6. XCELS: http://www.xcels.iapras.ru/; http://english.siom.cas.cn/rh/rp/201801/t20180126189619.html
7. N. N. Rozanov, "Four-wave interactions of intense radiation in vacuum," Zh. Eksp. Teor. Fiz. **103**(6), 1996–2007 (1993).

Optics EXPRESS

8. A. R. Bell and J. G. Kirk, "Possibility of Prolific Pair Production with High-Power Lasers," Phys. Rev. Lett. **101**(20), 200403 (2008).
9. R. Schützhold, H. Gies, and G. Dunne, "Dynamically Assisted Schwinger Mechanism," Phys. Rev. Lett. **101**(13), 130404 (2008).
10. S. S. Bulanov, V. D. Mur, N. B. Narozhny, J. Nees, and V. S. Popov, "Multiple Colliding Electromagnetic Pulses: A Way to Lower the Threshold of e + e- Pair Production from Vacuum," Phys. Rev. Lett. **104**(22), 220404 (2010).
11. T. M. Jeong, S. Weber, B. Le Garrec, D. Margarone, T. Mocek, and G. Korn, "Spatio-temporal modification of femtosecond focal spot under tight focusing condition," Opt. Express **23**(9), 11641–11656 (2015).
12. S. V. Bulanov, T. Z. Esirkepov, Y. Hayashi, M. Kando, H. Kiriyama, J. K. Koga, K. Kondo, H. Kotaki, A. S. Pirozhkov, S. S. Bulanov, A. G. Zhidkov, P. Chen, D. Neely, Y. Kato, N. B. Narozhny, and G. Korn, "On the design of experiments for the study of extreme field limits in the interaction of laser with ultrarelativistic electron beam," Nucl. Instrum. Methods Phys. Res., Sect. A **660**(1), 31–42 (2011).
13. P. Varga and P. Török, "Focusing of electromagnetic waves by paraboloid mirrors. I. Theory," J. Opt. Soc. Am. A **17**(11), 2081–2089 (2000).
14. S. S. Bulanov, T. Z. Esirkepov, A. G. R. Thomas, J. K. Koga, and S. V. Bulanov, "Schwinger limit attainability with extreme power lasers," Phys. Rev. Lett. **105**(22), 220407 (2010).
15. A. April and M. Piché, "4π Focusing of TM01 beams under nonparaxial conditions," Opt. Express **18**(21), 22128–22140 (2010).
16. I. Gonoskov, A. Aiello, S. Heugel, and G. Leuchs, "Dipole pulse theory: Maximizing the field amplitude from 4π focused laser pulses," Phys. Rev. A **86**(5), 053836 (2012).
17. I. M. Bassett, "Limit to Concentration by Focusing," Opt. Acta **33**(3), 279–286 (1986).
18. J. Handali, P. Shakya, and B. Barwick, "Creating electron vortex beams with light," Opt. Express **23**(4), 5236–5243 (2015).
19. X. Zhang, B. Shen, Y. Shi, X. Wang, L. Zhang, W. Wang, J. Xu, L Yi, and Z. Xu, "Generation of intense high-order vortex harmonics," Phys. Rev. Lett. **114**(17), 173901 (2015).
20. R. Nuter, P. Korneev, I. Thiele, and V. Tikhonchuk, "Plasma solenoid driven by a laser carrying an orbital angular momentum," Phys. Rev. E **98**(3), 033211 (2018).
21. A. M. Yao and M. J. Padgett, "Orbital angular momentum: origins, behavior and applications," Adv. Opt. Photonics **3**(2), 161–204 (2011).
22. D. G. Hall, "Vector-beam solutions of Maxwell's wave equation," Opt. Lett. **21**(1), 9–11 (1996).
23. Q. Zhan, "Cylindrical vector beams: from mathematical concepts to applications," Adv. Opt. Photonics **1**(1), 1–57 (2009).
24. J. A. Hoffnagle and C. M. Jefferson, "Design and performance of a refractive optical system that converts a Gaussian to a flattop beam," Appl. Opt. **39**(30), 5488–5499 (2000).
25. H. Ma, P. Zhou, X. Wang, Y. Ma, F. Xi, X. Xu, and Z. Liu, "Near-diffraction-limited annular flattop beam shaping with dual phase only liquid crystal spatial light modulators," Opt. Express **18**(8), 8251–8260 (2010).
26. E. Wolf, "Electromagnetic diffraction in optical systems I. An integral representation of the image field," Proc. R. Soc. Lond. A **253**(1274), 349–357 (1959).
27. I. S. Gradshteyn and I. M. Ryzhik, *Table of Integrals, Series, and Products* (Academic, 2007, p. 772).
28. T. M. Jeong, S. V. Bulanov, W. Yan, S. Weber, and G. Korn, "Generation of superposition modes by polarization-phase coupling in a cylindrical vector orbital angular momentum beam," OSA Continuum **2**(9), 2718–2727 (2019).
29. F. Rotermund and V. Petrov, "Generation of the fourth harmonic of a femtosecond Ti:sapphire laser," Opt. Lett. **23**(13), 1040–1042 (1998).
30. V. B. Berestetskii, E. M. Lifshitz, and L. P. Pitaevskii, *Quantum Electrodynamics* (Pergamon, 1982, chap. 10).
31. S. S. Bulanov, T. Z. Esirkepov, A. G. R. Thomas, J. K. Koga, and S. V. Bulanov, "Schwinger Limit Attainability with Extreme Power Lasers," Phys. Rev. Lett. **105**(22), 220407 (2010).
32. A. Gonoskov, I. Gonoskov, C. Harvey, A. Ilderton, A. Kim, M. Marklund, G. Mourou, and A. Sergeev, "Probing Nonperturbative QED with Optimally Focused Laser Pulses," Phys. Rev. Lett. **111**(6), 060404 (2013).
33. S. V. Bulanov, T. Esirkepov, and T. Tajima, "Light Intensification towards the Schwinger Limit," Phys. Rev. Lett. **91**(8), 085001 (2003).
34. I. J. Kim, K. H. Pae, C. M. Kim, H. T. Kim, H. Yun, S. J. Yun, J. H. Sung, S. K. Lee, J. W. Yoon, T. J. Yu, T. M. Jeong, C. H. Nam, and J. Lee, "Relativistic frequency upshift to the XUV regime using self-induced oscillatory flying mirrors," Nat. Commun. **3**(1), 1231 (2012).
35. T. Brabec and F. Krausz, "Intense few-cycle laser fields: Frontiers of nonlinear optics," Rev. Mod. Phys. **72**(2), 545–591 (2000).
36. S. V. Bulanov, T. Z. Esirkepov, M. Kando, A. S. Pirozhkov, and N. N. Rosanov, "Relativistic Mirrors in Plasmas–Novel Results and Perspectives," Phys.-Usp. **56**(5), 429–464 (2013).
37. S. S. Bulanov, A. Maksimchuk, A. G. Zhidkov, C. Schroeder, E. Esarey, and W. P. Leemans, "Relativistic spherical plasma waves," Phys. Plasmas **19**(2), 020702 (2012).
38. J. Koga, S. V. Bulanov, T. Esirkepov, M. Kando, S. S. Bulanov, and A. Pirozhkov, "Relativisitcally upshifted higher harmonic generation via relativistic flying mirrors," Plasma Phys. Controlled Fusion **60**(7), 074007 (2018).